



## Occurrence of albitite from Capo Malfatano, SW Sardinia: first report, characterization from mineralogy and whole-rock geochemistry

Gabriele Cruciani \*, Dario Fancello, Marcello Franceschelli

Department of Chemical and Geological Sciences, Cittadella Universitaria - 09042 Monserrato, Cagliari, Italy

### ARTICLE INFO

Submitted: November 2018

Accepted: January 2019

Available on line: January 2019

\* Corresponding author:  
gcrucian@unica.it

DOI: 10.2451/2019PM830

How to cite this article:  
Cruciani G. et al. (2019)  
Period. Mineral. 88, 19-31

### ABSTRACT

Within the sedimentary-volcanoclastic succession known as Bithia Unit (SW Sardinia) a decameter-wide albitite lens has been found and is here characterized from a geological, petrographic and geochemical point of view. Albitite is a yellowish, fine-grained body elongated and foliated according to the main schistosity of the hosting rocks (N20-25°-40°NW). The rock is made up by plagioclase porphyroclasts in a fine-grained matrix of plagioclase (up to 80%) and quartz; both porphyroclasts and small grains in matrix are almost pure albite (Ab<sub>98</sub>). Accessory phases are ilmenite, rutile, monazite, apatite and zircon. Bulk-rock chemical analyses show that the relative proportions of SiO<sub>2</sub>, Al<sub>2</sub>O<sub>3</sub> and Na<sub>2</sub>O strongly resemble those of pure albite. Major, trace and rare earth element (REE) contents strongly suggest geochemical affinity with the nearby Ordovician metavolcanics and orthogneiss from Capo Malfatano area described in literature. Furthermore, REE, Rb/Sr, Y/Ho and Zr/Hf ratios seem to exclude the involvement of a significant Na-rich fluid metasomatism.

Keywords: albitite; REE enrichment; Ordovician magmatism; SW Sardinia.

### INTRODUCTION

Albitites are uncommon rocks that occur in different geological scenarios. Most of them are linked to oceanic crust formation and thus can be found in rifting settings as well as in collisional settings within ophiolite complexes (Coleman and Peterman, 1975; Malpas, 1979; Gerlach et al., 1981; Flagler and Spray, 1991; Koepke et al., 2007; Li et al., 2013; Zeng et al., 2015). Albitites occur also in the late magmatic stages of plutons emplacement as the result of the interaction between Na-rich metasomatic fluids and granitic rocks (Mark, 1998; Castorina et al., 2006; Boulvais et al., 2007; Mohammad et al., 2007; Polito et al., 2009). Other occurrence of albitites are described in anorogenic settings where they represent plagioclase cumulus genetically linked to A-type granitoids (Azer et al., 2010). The multiplicity of geodynamic settings where albitites can be found in, has raised up the interest of many

authors and has led to several studies aimed to constrain their genesis. Furthermore, albitites are of great interest in ore geology given that metasomatic albitites are often associated to U, Th and REE-rich mineralization (Turpin et al., 1988; Polito et al., 2009; Singh et al., 2013; Wilde et al., 2013; Montreuil et al., 2015).

We characterize the Capo Malfatano albitite, here described for the first time, from a petrographic and geochemical point of view and we try to correlate them with the Ordovician igneous rocks widespread in the south-westernmost part of Sardinia. In addition, we make a geochemical comparison between the Capo Malfatano albitite and other albitites from different geodynamic settings with the aim to suggest some clues on the genetic processes that formed the Capo Malfatano albitites.

### GEOLOGICAL SETTING

The Paleozoic basement of Sardinia is a well-preserved

sector of the south European Variscan chain. Four tectono-metamorphic zones are commonly distinguished on the basis of deformation, structural framework and metamorphic grade (after Carmignani et al., 1994, 2001, and references therein): i) External Zone (foreland; southwestern Sardinia) made up by deformed parautochthonous rocks with a very low- to low-grade metamorphism; ii) External and iii) Internal Nappe Zones (Central to Northern Sardinia) that consist of a stacking of several tectonic units, whose metamorphic degree increases moving northward (Franceschelli et al., 1990) and towards the deepest units (Cruciani et al., 2016); iv) Axial (or Inner) Zone (Northern Sardinia) characterized by a rapid, northward increase of the metamorphic degree, from the green-schist to high pressure migmatite (Cruciani et al., 2014 a,b; Massonne et al., 2013; Fancello et al., 2018). The axial zone also extends in southern Corsica (Massonne et al., 2018). The Axial Zone has been further subdivided in two complexes separated by a regional-scale shear zone, the Posada-Asinara Line (PAL): the Low- to Medium-Grade Metamorphic Complex (L-MGMC, south of the PAL) and the High-Grade Metamorphic Complex (HGMC, north of the PAL). The HGMC mainly consists of sedimentary- and igneous-derived migmatites, rare marbles, tholeiitic and alkaline metabasite lenses with relics of eclogite facies (Cruciani et al., 2010, 2011) and layered amphibolites sequences resembling leptyno-amphibolite complexes (Franceschelli et al., 2005b). Retrogressed eclogite lenses are also found in the MGMC (Cruciani et al., 2015 a,b). Ordovician acidic calcalkaline intrusive and effusive rocks are distributed within the tectonic units from the foreland to the inner zone of the chain (Memmi et al., 1983; Oggiano et al., 2010; Gaggero et al., 2012; Cruciani et al., 2013). Variscan tectono-metamorphic events were accompanied by the emplacement of intrusive rocks belonging to the Sardinia batholith between 320-280 Ma (Casini et al., 2012, 2015). The metamorphic basement is unconformably covered by Late Carboniferous-Early Permian sedimentary rocks filling extensional basins (Carmignani et al., 1994; Barca et al., 1995). A detailed review on the geology and the tectonic-metamorphic evolution of the Variscan chain of Sardinia can be found in Carmignani et al. (2001), Ricci et al. (2004), Franceschelli et al. (2005a) and Cruciani et al. (2015c).

The Variscan metamorphic basement is made up by a succession of sediments and intercalated magmatic rocks belonging to three different magmatic cycles of Cambro-Ordovician ages (Oggiano et al., 2010; Gaggero et al., 2012). The first cycle ( $491.7 \pm 3.5$  and  $479.9 \pm 2.1$  Ma; U/Pb in zircon), hosted in the Cambro-Ordovician sedimentary succession, consists of transitional volcanic rocks ranging from intermediate to felsic. The second cycle of middle-Ordovician age ( $465.4 \pm 1.4$  Ma; U/Pb in

zircon) is characterized by a wide chemical variability that ranges from basalts to rhyolites and from calc-alkaline to sub-alkaline affinity. The intermediate to felsic extrusive products of this cycle are referred in literature as “porphyroids” (Auct.); they crop out mainly in the External Nappe Zone and to a lesser extent in the Inner Zone. The intrusive counterpart of the second cycle is represented by several plutons (now orthogneisses and migmatized orthogneisses) mainly outcropping in the Inner Zone. Radiometric ages for the protolith’s emplacement of these orthogneiss point to a middle-upper Ordovician: Lodè and Tanaunella  $456 \pm 14$  and  $458 \pm 7$  Ma, respectively (U/Pb in zircon; Helbing and Tiepolo, 2005); Golfo Aranci  $469 \pm 3.7$  Ma (U/Pb in zircon; Giacomini et al., 2006); Amphibole-bearing migmatite of Punta Sirenella Pb/Pb zircon age:  $452 \pm 3$  and  $461 \pm 12$  Ma (Pb/Pb in zircon; Cruciani et al., 2008). The third cycle ( $440 \pm 1.7$  Ma; U/Pb in zircon), related to a continental rifting geodynamic setting and to the collapse of the Mid-Ordovician volcanic arc (Oggiano et al., 2010), consists of metaepiclastites of alkalic affinity intercalated within the transgressive sedimentary sequence of post-Sandbian age (Caradocian transgression, Auct.), which mainly outcrop in the External Nappe Zone.

The southernmost part of the Sulcis area, near Capo Spartivento (Figure 1), is characterized by a complex geological and structural framework that is still a matter of debate. The sequence, from bottom to top, consists of Mt. Settiballas Micaschists, Mt. Filau Orthogneiss and Bithia Unit that, taken together, form the Southern Sulcis Complex (SSC; Carosi et al., 1998). This greenschist to amphibolite facies metamorphic complex is juxtaposed to anchizonal rocks belonging to the External Zone (foreland); from bottom to top, they are the Nebida Group, the Gonnese Group and the Iglesias Group (Pillola, 1991). The Nebida Group is a thick terrigenous sequence with minor layers of oolitic limestones dated at the Early Cambrian by means of Archeocyaths. The Gonnese Group consists of metadolostones and metalimestones belonging to a tidal flat environment that marks the transition from a siliciclastic to a carbonate-dominated depositional system. The Iglesias Group testifies an increase of sea deepness recorded by marly nodular limestones at the bottom (Campo Pisano Fm.) and phyllites and metasiltites/metasandstones at the top (Cabitzza Fm.) where these latter indicate the definitive drowning of the carbonate platform.

The contrast between the low-to medium-grade metamorphic rocks of the SSC and the adjacent anchizone metamorphic rocks has led to different interpretations of the geological history of this area. Former authors considered the SSC as a pre-Variscan metamorphic basement lying beneath the foreland sedimentary succession with a conformable or unconformable stratigraphic contact. Recent papers

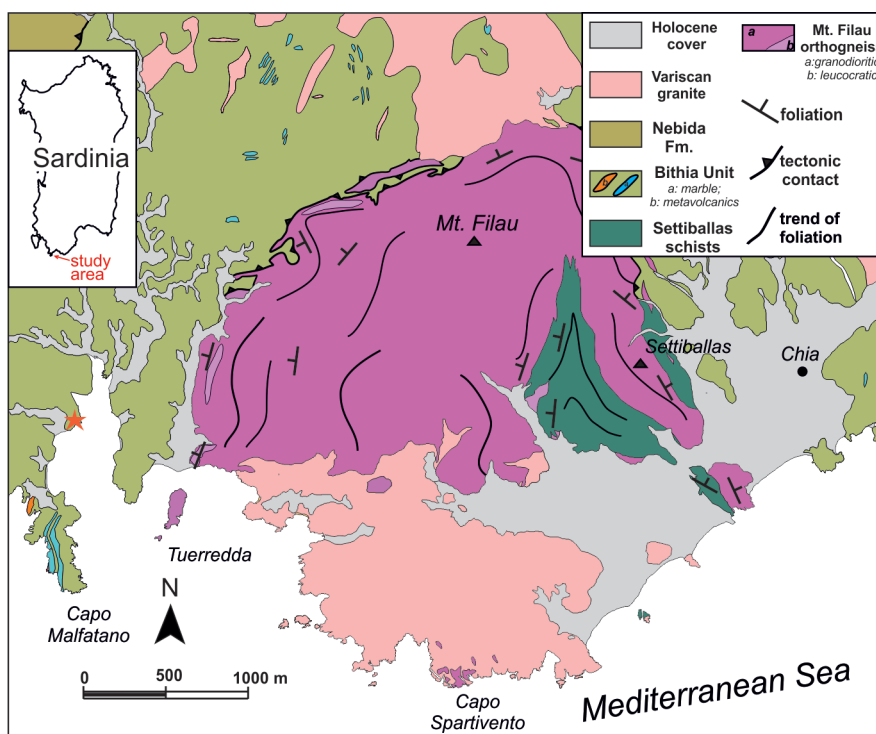


Figure 1. Geological sketch map of the study area (modified from Cruciani et al., 2019). The orange star indicates the position of the albitite outcrop. Inset shows location of the study area.

refuse this interpretation on the basis of new structural and geochronological data. Pavanetto et al. (2012), dated the metavolcanic rocks at  $457.01 \pm 0.17$  Ma and the Mt. Filau orthogneiss at  $458.21 \pm 0.32$  and  $457.50 \pm 0.33$  Ma (U/Pb in zircon) and suggested the allochthonous origin of the SSC (or at least a part of it) that could be a structural klippe belonging to the External Nappe Zone, thrust into its actual position during the late Variscan deformation stages. Similar U/Pb zircon age was provided by Cruciani et al. (2018) that dated metavolcanics from the Bithia Unit at  $462.1 \pm 4.3$  Ma (U/Pb in zircon). Nonetheless, other authors still support the former interpretation of the SSC as a pre-Variscan basement and indicate a pre-Cambrian age of the Bithia Fm. on the basis of *Archeocyatha*'s discovery (Costamagna, 2015; Costamagna et al., 2016); according to these authors, the radiometric ages detected in metavolcanics from Bithia Fm. are affected by Pb loss due to a later opening of the isotopic system.

#### FIELD OCCURRENCE

In the eastern side of the Capo Malfatano peninsula, within the Bithia Unit (Pavanetto et al., 2012), a small body of albitite (10 meter-wide and 50 meter-long) outcrops (Figure 1). It consists of a fine-grained, foliated, yellowish lens elongated according to the main schistosity (Figure 2a). A centimeter-sized alternation of lighter and darker

layers is visible in some portions of the outcrop, whereas in other parts the aspect is more massive and homogeneous. Millimeter-sized, rounded plagioclase, visible at the naked eye, are dispersed in a fine-grained matrix. The pervasive foliation,  $N20-25^{\circ}-40^{\circ}NW$ , is parallel to the elongation of the lens and to the foliation of the hosting rocks (Figure 2b). Pavanetto et al. (2012) considered this foliation formed during the Variscan orogeny and in particular tied to the Sarrabus Variscan phase. On the XY plane a weak mineralogical lineation  $N135^{\circ}-30^{\circ}NW$  is marked by the phyllosilicates. Centimeter-thick veins made up of quartz and reddish-brown oxides, subparallel to the foliation are commonly found. The surrounding rocks, belonging to the Bithia Unit, consist of low-grade metarkose and phyllites. Beneath the lens they are light-colored and coarse-grained resembling metarkoses or metaepiclastites, whereas at the top of the lens they are characterized by a finer grain-size and a darker color due to the higher amount of micas (phyllites). The contact between the albitite lens and the Bithia Unit is covered by soil and vegetation but is supposed to be concordant due to the same foliation in both rocks and to the elongation direction of the albitite, parallel to this foliation.

#### ANALYTICAL METHODS

Microstructural study and BSE imaging on albitite

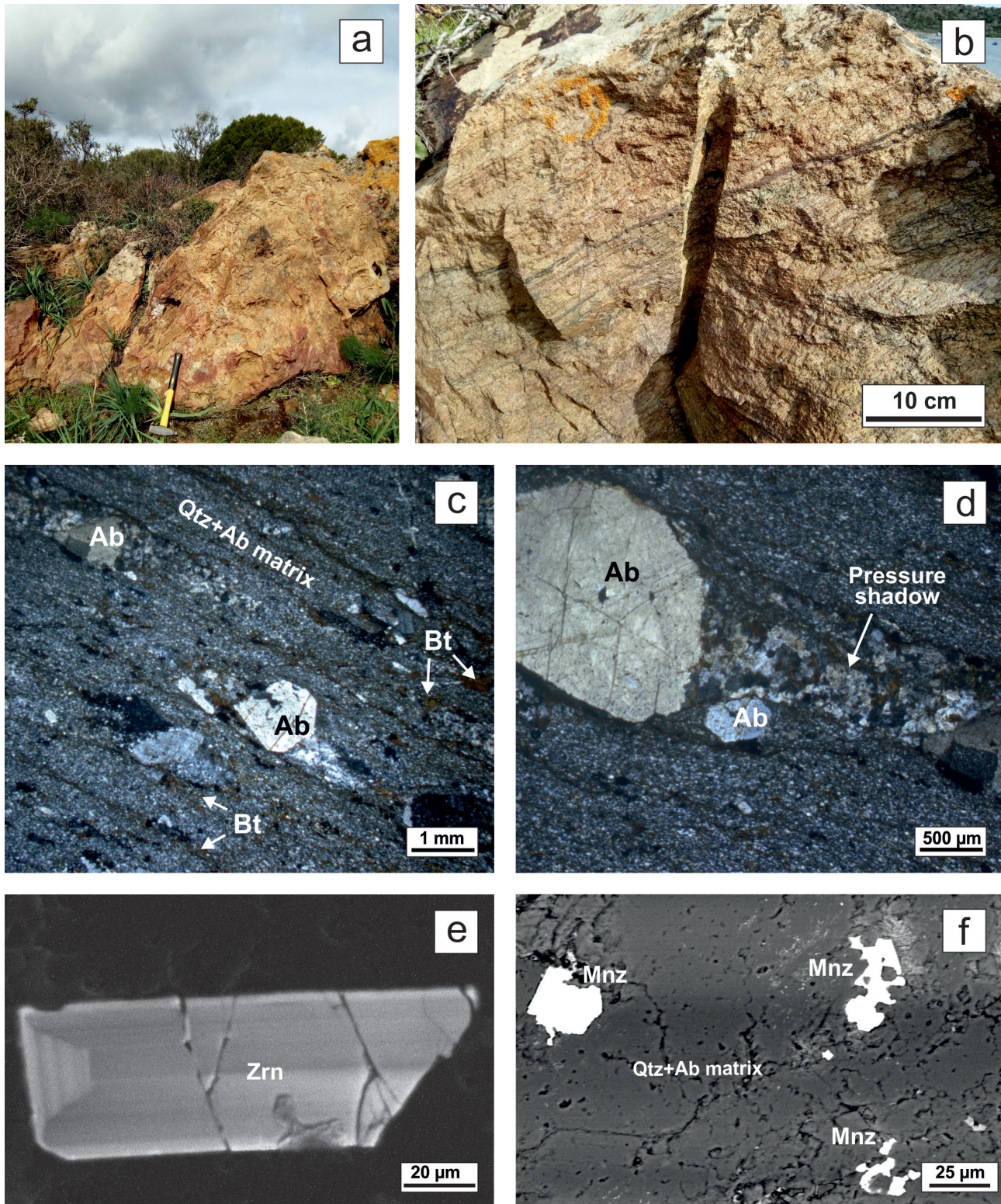


Figure 2. a) Field appearance of albitite lens from Capo Malfatano; b) detail of the outcrop showing alternating yellowish and dark layers which identify the rock foliation; c) photomicrograph of CM6 sample consisting of albite porphyroclasts in a fine-grained Ab+Qtz matrix; d) detail of pressure shadow on the side of a plagioclase porphyroclasts; e) cathodoluminescence image of zircon with concentric zoning; f) BSE image of a monazite aggregate in CM6 sample. Mineral abbreviations as in Fettes and Desmons (2007).

samples were performed with a FEI Quanta 200 scanning electron microscope (SEM) equipped with an EDAX-EDS detector at Centro Servizi di Ateneo per la Ricerca (CeSAR) of Cagliari University. The major-element composition of plagioclase, biotite, chlorite and some selected trace elements (La, Ce, Pr, Nd, Sm, Zr, Pb, U, Th, Y, Hf) in zircon and monazite were determined with a fully automated JEOL 8200 Super Probe at the Dipartimento di Scienze della Terra “Ardito Desio” University of Milano. Operating conditions were 15 kV accelerating voltage, beam current of 15 nA and 5-10  $\mu\text{m}$  variable spot size. Natural and synthetic wollastonite, olivine, corundum, magnetite, rutile, orthoclase, jadeite, pure Mn, pure Cr, fluoro-phlogopite and barite were used as standards. Zircon analyses were performed with beam current and spot size 5 nA and 1  $\mu\text{m}$  respectively, with the following standards: zircon, galena,  $\text{ThO}_2$ ,  $\text{UO}_2$ , grossular and REE-phosphate.

Table 1. Representative microprobe analyses and structural formulae of albite, biotite and chlorite of albitite sample CM6 from Capo Malfatano.

	Ab	Ab	Bt	Chl
$\text{SiO}_2$	68.77	68.84	36.34	29.52
$\text{Al}_2\text{O}_3$	19.45	19.39	18.45	18.24
FeO	-	-	28.02	35.60
MnO	-	-	-	0.19
MgO	-	-	2.95	5.13
CaO	0.27	0.12	0.28	0.11
$\text{Na}_2\text{O}$	11.43	11.53	0.91	0.18
$\text{K}_2\text{O}$	0.08	0.12	8.22	0.22
Total	100.00	100.00	95.17	89.19
Oxy	8	8	22	28
Si	3.001	3.004	5.729	6.392
Al	1.000	0.997	3.429	4.656
$\text{Fe}^{2+}$	-	-	3.694	6.447
Mn	-	-	-	0.035
Mg	-	-	0.693	1.656
Ca	0.013	0.006	0.047	0.026
Na	0.967	0.975	0.278	0.076
K	0.004	0.007	1.653	0.061
Total	4.985	4.989	15.523	19.348
XMg	-	-	0.16	0.20
XAb	0.99	0.99	-	-
XOr	0.00	0.01	-	-

Three selected albitite samples (CM5,6,7) were analyzed for major elements (XRF after lithium borate fusion) and trace elements (ICP-MS after lithium borate fusion and subsequent four acid digestion) at ALS-Chemex Laboratories (Sevilla, Spain).

#### PETROGRAPHY AND MINERAL CHEMISTRY

The albitite consists of a very fine-grained (<100  $\mu\text{m}$ ), homogeneous matrix mainly made up of plagioclase (up to 90 vol.%), quartz and Fe-Ti oxides. Large, strongly altered biotite and a little amount (2-3 vol.%) of plagioclase porphyroclasts (up to 2 mm) are commonly observed within the matrix (Figure 2c). At the microscopic scale, the rock foliation is identified by the irregular alternation of light-colored quartz-feldspathic layers and darker mica-rich layers, by the alignment of biotite and chlorite in thin trails (Figure 2c) and locally by the elongation of albite porphyroclasts. The porphyroclasts commonly show pressure shadows formed by fine-grained quartz and albite (Figure 2d). Plagioclase, both porphyroclasts and little grains in the matrix, have a constant composition, very close to the albite end-member ( $\text{Ab}_{99}$ ); even the larger grains do not show chemical zonation. Biotite composition is  $X_{\text{Mg}}=0.16$  and  $\text{Al}^{\text{IV}}=2.27$ . On the basis of the  $X_{\text{Fe}}$  vs  $\text{Al}^{\text{IV}}$  diagram by Deer et al. (1992) the studied biotite can be classified as aluminium-annite. Chlorite ( $X_{\text{Mg}}=0.20$ ) is rarely found as a pure phase in patches within large chloritized biotite (Table 1). Zircon occurs in euhedral to anhedral crystals ranging in size between 50 and 120  $\mu\text{m}$ . Euhedral zircon grains show the typical concentric zoning of igneous origin (Figure 2e). However, no systematic variation of the trace elements has been observed between core and rim.  $\text{La}_2\text{O}_3$  and  $\text{Ce}_2\text{O}_3$  in zircon are up to 0.033 and 0.169 wt% (corresponding to La 281 and Ce 1443 ppm), respectively, whereas medium-REE elements (i.e.  $\text{Nd}_2\text{O}_3$  and  $\text{Sm}_2\text{O}_3$ ) are in the range 0.022-0.029 and 0.006-0.110 wt% (i.e. 189-249 and 52-949 ppm). Thorium, Yttrium, Uranium and Hafnium are within the following ranges (wt%):  $\text{ThO}_2$ : 0.021-0.060;  $\text{Y}_2\text{O}_3$ : 0.015-0.172;  $\text{UO}_2$ : 0.009-0.173;  $\text{HfO}_2$ : 0.759-1.310. Th/U ratios of zircon are in the range 0.3 to 0.6 in both core and rim (Table 2), similar to values observed in magmatic zircon (Rubatto and Hermann, 2007). Monazite crystals are commonly anhedral, with corroded rims and locally porous texture. Monazite can be found in single grains, sometimes associated with rutile and chlorite or in aggregate up to 0.5 mm in size in the matrix (Figure 2f).  $\text{UO}_2$  in monazite is up to 0.04 wt%.  $\text{Y}_2\text{O}_3$  ranges between 0.365 and 0.938 wt%,  $\text{ThO}_2$  between 0.356 and 0.849 wt% (Table 2). Ilmenite and rutile are found close to or within the altered biotite as well as in the albite and quartz matrix; locally they form rounded clusters up to 0.5 mm made up by small needles or anhedral grains. Apatite was also observed as accessory phase.

Table 2. Trace element composition of some selected zircon and monazite grains from sample CM6.

	Zircon					Monazite	
	Zr1-cor	Zr1-rim	Zr2	Zr3	Zr4	Mnz1	Mnz2
P <sub>2</sub> O <sub>5</sub>	0.377	0.380	0.365	0.347	0.342	30.70	31.42
SiO <sub>2</sub>	33.92	34.15	33.69	34.02	34.15	0.162	0.298
ZrO <sub>2</sub>	66.09	67.05	65.42	66.03	65.58	-	-
HfO <sub>2</sub>	0.998	1.036	1.090	1.095	0.759	-	-
ThO <sub>2</sub>	0.060	-	0.057	0.008	0.021	0.356	0.849
UO <sub>2</sub>	0.173	0.049	0.102	0.019	0.059	0.046	-
Y <sub>2</sub> O <sub>3</sub>	0.171	0.172	0.015	0.042	0.147	0.365	0.938
La <sub>2</sub> O <sub>3</sub>	0.033	-	0.015	-	-	16.88	14.78
Ce <sub>2</sub> O <sub>3</sub>	0.098	0.027	0.034	-	0.169	33.86	33.60
Pr <sub>2</sub> O <sub>3</sub>	0.047	0.011	0.096	0.068	0.103	2.66	3.02
Nd <sub>2</sub> O <sub>3</sub>	-	0.022	-	-	0.029	13.49	12.28
Sm <sub>2</sub> O <sub>3</sub>	-	-	0.110	0.010	0.006	2.13	2.32
CaO	-	-	0.038	0.033	0.050	0.077	0.230
Total	101.97	102.90	101.03	101.67	101.42	100.73	99.74
Th/U	0.35	-	0.56	0.42	0.36	7.73	-

### BULK ROCK CHEMISTRY

The three samples reported in Table 3 and Figure 3 show a very similar chemical composition. Main oxides are SiO<sub>2</sub> 65.13-65.56 wt%, Al<sub>2</sub>O<sub>3</sub> 17.60-17.69 wt%, Na<sub>2</sub>O 8.39-9.00 wt% and Fe<sub>2</sub>O<sub>3</sub> 3.83-4.58 wt%. Minor amounts of TiO<sub>2</sub> 0.48-0.59 wt%, MgO 0.20-0.40 wt%, CaO 0.15-0.29 wt%, K<sub>2</sub>O 0.18-0.23 wt%, P<sub>2</sub>O<sub>5</sub> 0.14-0.26 wt% and MnO 0.03-0.05 wt% are also present. LOI ranges between 1.87-2.33 wt%. The most striking geochemical features are the very high sodium content and the relative proportions of SiO<sub>2</sub>, Al<sub>2</sub>O<sub>3</sub> and Na<sub>2</sub>O that strongly resemble those of pure albite. The relatively high iron and titanium contents together with LOI values suggest the former presence of biotite, now altered in Fe-Ti oxides. The very low CaO and K<sub>2</sub>O contents suggest scarce amounts of anorthite component in plagioclase and of K-feldspar, respectively. The CIPW normative minerals (Table 3) confirm this assumption and show albite content of 73-78 wt%, quartz 10-13 wt% and orthoclase 1.1-1.6 wt%. Normative anorthite is absent, or very low (0.42 wt% in one sample out of three). All samples are corundum, magnetite, ilmenite and hyperstene normative.

Trace and rare earth elements (REE) composition of the analyzed samples is given in Table 3. All samples show low Sr and Ba contents (57.7-76.5 ppm and 76.4-148.0 ppm, respectively) and very low Rb contents (3.8-5.7 ppm). In the Ba-Rb-Sr diagram of Figure 4, the Capo Malfatano albitite is compared with metavolcanic rocks

from Cruciani et al. (2018), Ordovician orthogneiss from Cruciani et al. (2019), back-arc related cumulate albitites from Zeng et al. (2015), A-type related cumulate albitite from Azer et al. (2010), metasomatic albitite from Castorina et al. (2006), and with metasomatic albitite from Boulvais et al. (2007). In this diagram, the studied albitite is characterized by low Rb content and plot near to the albitites described by Zeng et al. (2015) whereas the Bithia metavolcanics (Cruciani et al., 2018) and the Mt. Filau orthogneiss (Cruciani et al., 2019) plot parallel to the Ba-Rb side, typical of granite and strongly differentiate granites (El Bouseily and El Sokkary, 1975). The diagram in Figure 5a shows patterns characterized by negative anomalies of Rb, Ba, K, Sr and Ti. Zr content is quite high (633-682 ppm) as well as, Nb (21.5-25.3 ppm), Hf (15.8-19.2 ppm), Th (23.6-33.4 ppm) and total REE (350-424 ppm). Zr/Hf and Nb/Ta are not fractionated with respect to chondrite thus falling in the CHARAC field proposed by Bau (1996). REE patterns of albitite samples (Figure 5c) are characterized by the enrichment in LREE, the negative Eu anomaly and a moderately fractionated pattern (Ce<sub>N</sub>/Yb<sub>N</sub>=4.95-5.43) especially of LREE, whereas the HREE mark an almost flat trend (Gd<sub>N</sub>/Yb<sub>N</sub>=1.57-1.64).

### DISCUSSION

#### Comparison of albitite with Ordovician metavolcanics and orthogneiss from Capo Malfatano

The Capo Malfatano albitite shares its structural

Table 3. Major element composition (wt%) and CIPW norm (vol%) of three selected albitite samples from Capo Malfatano.

Sample	CM5	CM6	CM7
SiO <sub>2</sub>	65.56	65.13	65.28
TiO <sub>2</sub>	0.59	0.48	0.54
Al <sub>2</sub> O <sub>3</sub>	17.60	17.69	17.60
Fe <sub>2</sub> O <sub>3</sub>	3.83	4.41	4.58
MnO	0.05	0.03	0.06
MgO	0.20	0.40	0.36
CaO	0.29	0.15	0.26
Na <sub>2</sub> O	9.00	8.83	8.39
K <sub>2</sub> O	0.23	0.18	0.27
P <sub>2</sub> O <sub>5</sub>	0.26	0.24	0.14
LOI	2.23	1.87	2.33
Tot	99.87	99.45	99.85
Qtz	10.48	10.52	12.80
Or	1.42	1.12	1.65
Ab	78.27	76.92	73.11
An	-	-	0.42
C	2.61	3.05	3.46
Hy	4.65	6.08	6.15
Mt	0.86	0.99	1.03
Ilm	1.16	0.93	1.06
Ap	0.63	0.58	0.32

features with the host Bithia Unit, thus it is likely that both rocks were affected by the same Variscan metamorphic deformation events. According to Costamagna et al. (2016), early to late Carboniferous Variscan orogenesis resulted in low-temperature ( $T \approx 300$  °C) and low-pressure ( $P = 0.25$  GPa) metamorphism and the development of folds and thrusts in the Bithia Unit. The possible role of metamorphism must be evaluated when attempting to decipher the genesis of this rock. In the greenschist facies, plagioclase composition tends to be modified toward albite component; it could be argued that the low-grade metamorphism modified the composition of an original Ca-rich plagioclase in the cumulus leading to the current albite composition. But, if so, some Ca-rich phase (such as epidote or titanite) produced by the Ca releasing from plagioclase should have formed and this is not the case. Thus, the Variscan effect is probably reflected just by grain size reduction and foliation development whereas it is unlikely that significant chemical-mineralogical modification occurred in this rock.

The geochemical features of albitites from Capo Malfatano are here compared with those of Ordovician orthogneisses (after Cruciani et al., 2019) and metavolcanics rocks (from Cruciani et al., 2018) outcropping in the same area. Correlation diagrams of major oxides against silica (Figure 3) show different behaviors; Al<sub>2</sub>O<sub>3</sub>, Fe<sub>2</sub>O<sub>3</sub> and TiO<sub>2</sub> are negative related to silica in all samples (albitite, orthogneiss and metavolcanics). On the contrary, Na<sub>2</sub>O and K<sub>2</sub>O whose content is quite constant in both metavolcanics and

Table 3. Continued: Trace and rare earth elements (ppm) and Zr/Hf, Y/Ho ratios of three selected albitite samples. -: below detection limit.

Sample	CM5	CM6	CM7
V	27	43	71
Zn	-	61	34
Co	-	2.1	2.2
Ga	26.8	32.2	32.8
Rb	5.0	3.8	5.7
Sr	57.7	64.3	76.5
Y	74	71	88
Zr	670	633	682
Nb	23.3	21.5	25.3
Sn	8	9	8
Cs	0.49	0.55	0.5
Ba	76.4	148	107.5
Hf	15.8	16.9	19.2
Ta	1.5	1.8	2.1
W	3	5	5
Pb	-	8	7
Th	23.6	28.5	33.4
U	6.04	6.63	6.54
La	67.6	72.9	83.1
Ce	135	147	162
Pr	17.1	19.3	21.6
Nd	66.3	68.6	77.5
Sm	13.45	14.15	16.75
Eu	1.63	1.51	1.66
Gd	14.05	14.95	17.5
Tb	2.22	2.28	2.76
Dy	12.8	13.4	16.6
Ho	2.68	2.74	3.36
Er	7.96	7.99	9.6
Tm	1.11	1.22	1.48
Yb	7.40	7.52	9.06
Lu	1.05	1.22	1.45
ΣREE	350	375	424
Zr/Hf	42.41	37.46	35.52
Y/Ho	27.57	25.84	26.07

orthogneiss, are not related to silica; in these diagrams, albitite can be easily distinguished due to the high Na<sub>2</sub>O and low K<sub>2</sub>O content. CaO do not shows any correlation with SiO<sub>2</sub> in the studied albitite, whereas it shows negative correlation with SiO<sub>2</sub> in the orthogneiss. The Harker's diagrams of Figure 3 show a continuous evolution trend for Al<sub>2</sub>O<sub>3</sub> and TiO<sub>2</sub>, from albitite to metavolcanics and orthogneiss.

Spider and REE diagrams further suggest the geochemical affinity of albitite with neighboring metavolcanics and orthogneiss. Figures 5 a,b show that all reported rocks have a similar calcalkaline signature even if with some noticeable differences (Rb depletion, absence of Pb positive anomaly). REE patterns of Capo Malfatano are also similar to those observed in both metavolcanics and orthogneiss (Figure 5d) even if albitite has higher REE contents.

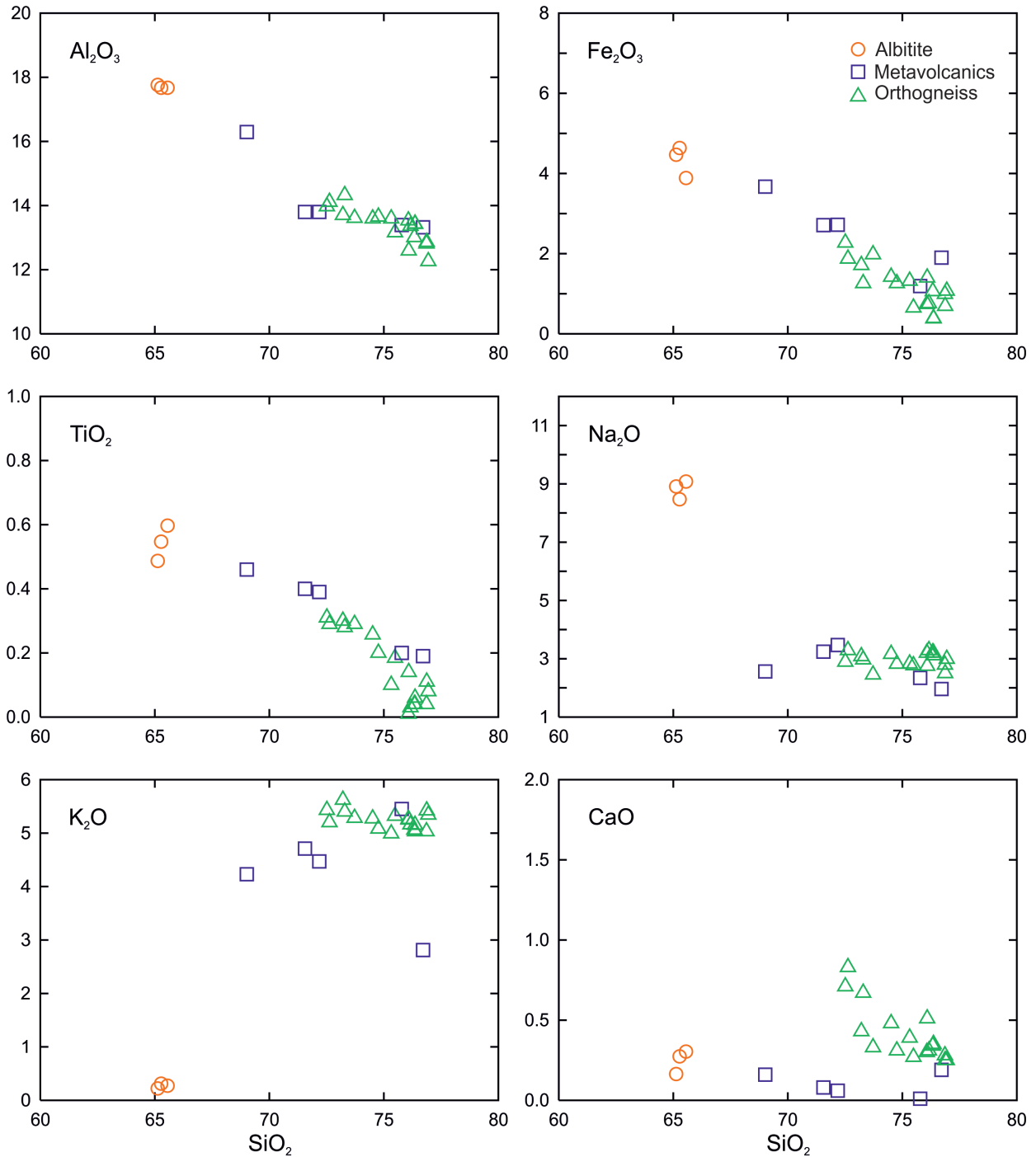


Figure 3. Harker's diagrams showing the correlation between major oxides and silica in albitite samples from Capo Malfatano, compared with Ordovician orthogneiss (from Cruciani et al., 2019) and metavolcanic rocks (from Cruciani et al., 2018) that outcrop in the same area.

A significant feature of Capo Malfatano albitite is the Zr content noticeably higher than in the other Ordovician igneous rocks. The Th/U ratios in zircon seem to suggest an igneous origin of this mineral, also supported by the slight concentric zoning observed in zircon grains (Figure 2e).

K/Rb ratio tends to decrease with metasomatism and fluids influx; Shaw (1968) and Dostal and Chatterjee (1995, 2000) suggest a threshold of  $K/Rb < 150$  as an index of the involvement of mineralizing fluids in the late magmatic phases. The Capo Malfatano albitite has

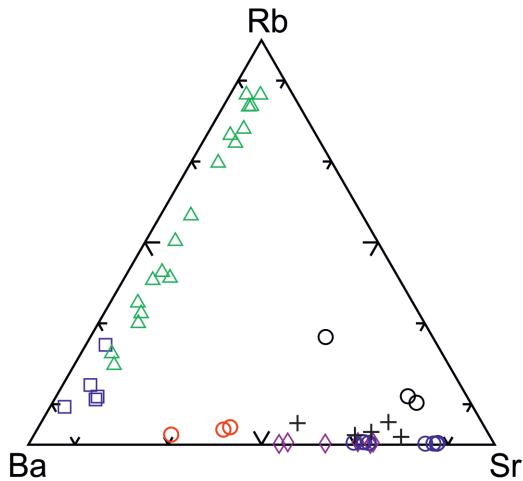


Figure 4. Ba-Rb-Sr diagram showing red circle: albitite samples from this study; blue square: metavolcanic rocks (from Cruciani et al., 2018); green triangle: Ordovician orthogneiss (from Cruciani et al., 2019); pink lozenges: back-arc related cumulate albitites from Zeng et al. (2015); black crosses: A-type related cumulate albitite from Azer et al. (2010); blue circles: metasomatic albitite from Castorina et al. (2006); black circles: metasomatic albitite from Boulvais et al. (2007).

a K/Rb ranging between 382 and 393 thus quite far than the abovementioned threshold. Furthermore, K/Rb vs Rb shows a negative trend within igneous derived rocks of Capo Malfatano suggesting a continuous evolution trend. Also Zr/Hf and Y/Ho ratios can provide some information about the possible fluids involvement. A modification in Zr/Hf and Y/Ho ratios occurs when fluids are involved in diagenetic, metamorphic or metasomatic processes. The Capo Malfatano albitites are characterized by Zr/Hf and Y/Ho very close to the chondrite values (Figure 6a) similarly to the most part of orthogneiss and metavolcanics samples.

#### Comparison with albitites from different geodynamic settings

The albitite from Capo Malfatano is here compared with other albitites from different geological environments such as: i) metasomatism processes (Castorina et al., 2006; Boulvais et al., 2007); ii) cumulate of plagioclase from A-type granites (Azer et al., 2010); iii) plagiogranites formed in a subduction setting in an oceanic back-arc basin (Zeng et al., 2015). In the Ba-Rb-Sr diagram of Figure 4 both cumulate albitites belonging to A-type granite and back arc-related plagiogranite fall near to the

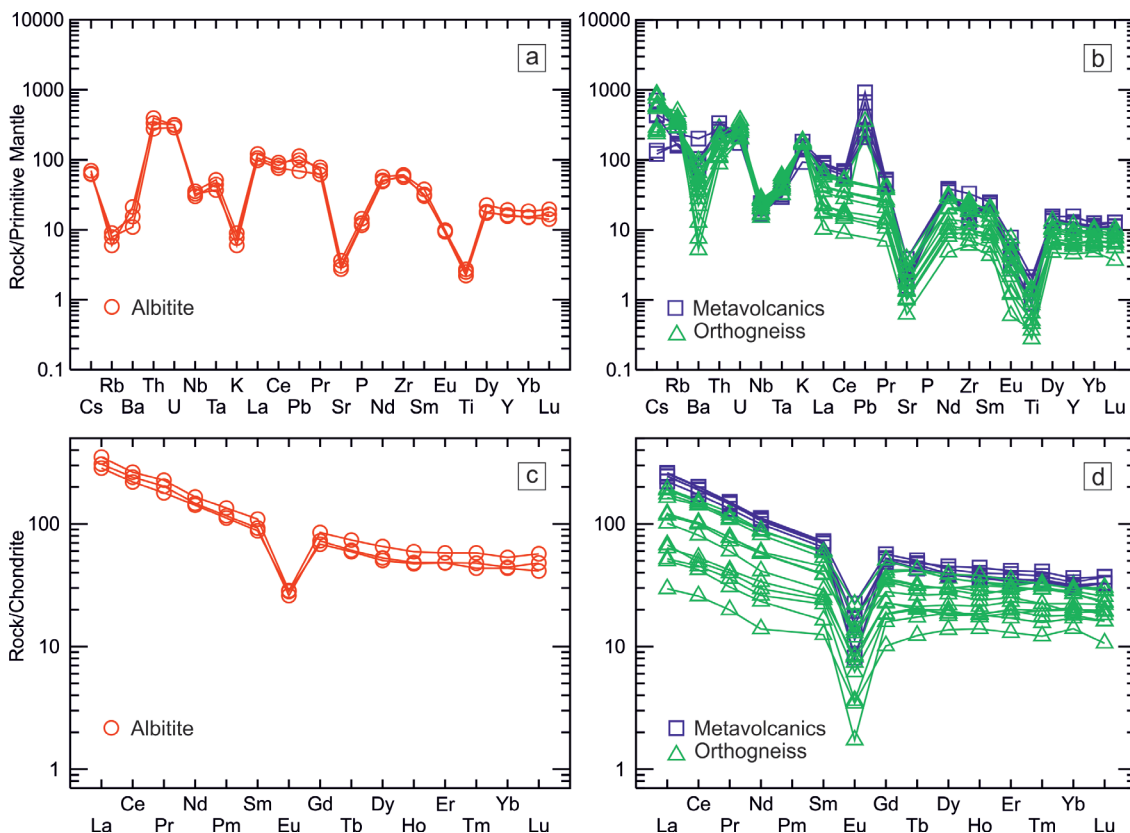


Figure 5. Spider diagrams of Capo Malfatano albitite (a) and orthogneiss and metavolcanics from Capo Malfatano area (b) normalized to the primitive mantle; REE patterns of albitite (c) and orthogneiss and metavolcanics (d) normalized to the chondrite. Orthogneiss and metavolcanics analyses are from Cruciani et al. (2019) and Cruciani et al. (2018), respectively. Normalization according to Sun and McDonough (1989).

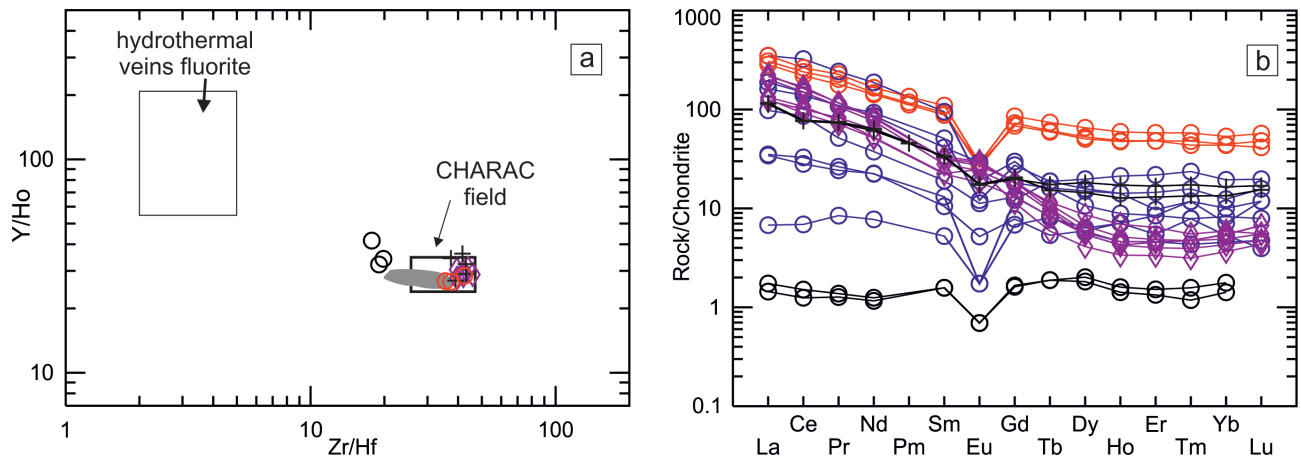


Figure 6. Comparison between albitite from Capo Malfatano and different albitite bodies reported in literature: a) Y/Ho vs Zr/Hf diagram; b) REE patterns normalized to the chondrite (according to Sun and McDonough, 1989). Symbols as in Figure 4 except greyish area representing orthogneiss from Capo Malfatano (Cruciani et al., 2019). CHARAC field represents trace element behavior controlled by charge and radius (Bau, 1996).

Sr apex, suggesting their affinity to a source less evolved than that of Capo Malfatano albitite. Metasomatic albitite also plot close to the Sr apex but this fact is not totally reliable due to the strong effect of metasomatism in the mobilization of Ba and Sr.

The metasomatism effect is well shown by the Y/Ho vs Zr/Hf diagram (Figure 6a). Indeed, all albitites produced by cumulate fall in the CHARAC field, close to the chondrite values, irrespective of their source. On the contrary, albitites produced by Na-metasomatism fall outside this range, closer to the ratios of fluorite in hydrothermal veins. Metasomatic albitite from Orani (Castorina et al., 2006) are not reported because Hf was not analyzed by these authors, but Y/Ho ratio are lower than the CHARAC range (24-34).

REE patterns (Figure 6b) show quite different behavior among the different types of albitite. As above described, Capo Malfatano albitite is characterized by a moderate fractionation of LREE, a negative Eu anomaly and an almost flat trend of HREE. Albitite originated in a back-arc related environment (Zeng et al., 2015) shows strongly fractionated pattern resulting in a steep slope from LREE to HREE separated by slightly positive Eu anomaly. REE patterns of albitite from the anorogenic setting (Azer et al., 2010) are similar to those of Capo Malfatano albitite, but with lower absolute content in almost all REE except the Eu (three samples showing anomalous signature due to crystal fractionation of REE-bearing phases where excluded from the comparison). Albitites produced by Na-metasomatism are characterized by a very wide range of REE contents and by different shapes, thus is difficult to make a significant comparison with the other types of albitite. However, some general consideration

can be done; i) most of samples have lower REE contents compared to the previously described albitites, and those reported by Boulvais et al. (2007) are the lowest; ii) LREE are strongly to slightly fractionated and show a wide variability in absolute contents; iii) HREE define an almost flat trend and their content is less variable as compared to LREE; iv) all samples have a more or less marked Eu negative anomaly whose intensity is independent from the concentration of the other REE. In summary, all these evidences seem to exclude the involvement of a significant Na-metasomatism during the Capo Malfatano albitite formation.

#### CONCLUDING REMARKS

Field survey together with mineralogical, petrographical and geochemical characterization of albitite body from Capo Malfatano led to the following main conclusions:

- Albitite from Capo Malfatano is a yellowish, fine-grained, foliated rock characterized by albite-rich matrix (Ab > 80 vol%) and millimeter-sized albite porphyroclasts with a geochemical signature similar to Ordovician orthogneiss and metavolcanics from the same area. The albitite microstructure was probably acquired during the main Variscan deformation phase that led to the grain size reduction.

- The Capo Malfatano albitite does not easily correlate with other albitites of igneous and metasomatic origin described in literature.

- Trace and rare earth elements contents suggest that the albitite underwent negligible, or even absent, fluid involvement (i.e. metasomatic processes are not significant). This is also supported by the absence of any metasomatic-type texture. On the other hand geochemical

data do not allow to define a igneous origin for the Capo Malfatano albitite. The only evidence in favour of igneous origin is the association in space and, probably, in time with Ordovician metaigneous rocks of Bithia Unit, the igneous origin of the zircon as well as the calcalkaline affinity of the rock.

#### ACKNOWLEDGEMENTS

The authors are grateful to Reviewer Aida Maria Conte that improved the final version of the manuscript. Financial support was provided by Università di Cagliari and FdS-RAS funding F72F16003080002.

#### REFERENCES

- Azer M.K., Stern R.J., Kimura J.I., 2010. Origin of a late Neoproterozoic (605±13 Ma) intrusive carbonate-albitite complex in Southern Sinai, Egypt. *International Journal of Earth Sciences* 99, 245-267.
- Barca S., Carmignani L., Eltrudis A., Franceschelli M., 1995. Origin and evolution of the Permian-Carboniferous basin of Mulargia Lake (South-Central Sardinia, Italy) related to the Late-Hercynian extensional tectonic. *Comptes Rendus de l'Académie des Sciences Paris* 321 (IIa), 171-178.
- Bau M., 1996. Controls on the fractionation of isovalent trace elements in magmatic and aqueous systems: evidence from Y/Ho, Zr/Hf, and lanthanide tetrad effect. *Contributions to Mineralogy and Petrology* 123, 323-333.
- Boulvais P., Ruffet G., Cornichet J., Mermet M., 2007. Cretaceous albitization and dequartzification of Hercynian peraluminous granite in the Salvezines Massif (French Pyrénées). *Lithos* 93, 89-106.
- Carmignani L., Carosi R., Di Pisa A., Gattiglio M., Musumeci G., Oggiano G., Pertusati P.C., 1994. The hercynian chain in Sardinia (Italy). *Geodinamica Acta* 7, 31-47.
- Carmignani L., Oggiano G., Barca S., Conti P., Salvadori I., Eltrudis A., Funedda A., Pasci S., Salvadori I., 2001. Geologia della Sardegna. Note illustrative della Carta Geologica della Sardegna in scala 1: 200.000. *Memorie Descrittive della Carta Geologica d'Italia* 60, 283 pp.
- Carosi R., Perillo M., Pertusati P.C., 1998. Structural evolution of the Southern Sulcis metamorphic complex (SW Sardinia, Italy). *Comptes Rendus de l'Académie des Sciences-Series IIA-Earth and Planetary Science* 326, 505-512.
- Casini L., Cuccuru S., Maino M., Oggiano G., Tiepolo M., 2012. Emplacement of the Arzachena Pluton (Corsica-Sardinia Batholith) and the geodynamics of incoming Pangaea. *Tectonophysics* 544-545, 31-49.
- Casini L., Cuccuru S., Puccini A., Oggiano G., Rossi Ph., 2015. Evolution of the Corsica-Sardinia Batholith and late-orogenic shearing of the Variscides. *Tectonophysics* 646, 65-78.
- Castorina F., Masi U., Padalino G., Palomba M., 2006. Constraints from geochemistry and Sr-Nd isotopes for the origin of albitite deposits from Central Sardinia (Italy). *Mineralium Deposita* 41, 323-338.
- Coleman R.G. and Peterman Z.E., 1975. Oceanic plagiogranite. *Journal of Geophysical Research* 80, 1099-1108.
- Costamagna L.G., 2015. The Capo Malfatano metaconglomerates in the Early Cambrian of SW Sardinia, Italy: key level for a new stratigraphic setting and evidence of Cadomian tectonics. *Zeitschrift der Deutschen Gesellschaft für Geowissenschaften* 166, 21-33.
- Costamagna L.G., Elter F.M., Gaggero L., Mantovani F., 2016. Contact metamorphism in Middle Ordovician arc rocks (SW Sardinia, Italy): New paleogeographic constraints. *Lithos* 264, 577-593.
- Cruciani G., Dini A., Franceschelli M., Puxeddu M., Utzeri D., 2010. Metabasite from the Variscan belt in NE Sardinia, Italy: within-plate OIB-like melts with very high Sr and low Nd isotope ratios. *European Journal of Mineralogy* 22, 509-523.
- Cruciani G., Fancello D., Franceschelli M., Musumeci G., 2019. Geochemistry of the Monte Filau orthogneiss (SW Sardinia, Italy): insight into the geodynamic setting of Ordovician felsic magmatism in the N/NE Gondwana margin. *Italian Journal of Geosciences* 138, 136-152.
- Cruciani G., Fancello D., Franceschelli M., Scodina M., Spano M.E., 2014a. Geothermobarometry of Al-silicate bearing migmatites from the Variscan chain of NE Sardinia, Italy: a P-T pseudosection approach. *Periodico di Mineralogia* 83, 19-40.
- Cruciani G., Franceschelli M., Foley S.F., Jacob D.E., 2014b. Anatectic amphibole and restitic garnet in Variscan migmatite from NE Sardinia, Italy: insights into partial melting from mineral trace elements. *European Journal of Mineralogy* 26, 381-395.
- Cruciani G., Franceschelli M., Groppo C., 2011. P-T evolution of eclogite-facies metabasite from NE Sardinia, Italy: insights into the prograde evolution of Variscan eclogites. *Lithos* 121, 135-150.
- Cruciani G., Franceschelli M., Groppo C., Oggiano G., Spano M.E., 2015a. Re-equilibration history and P-T path of eclogites from Variscan Sardinia, Italy: A case study from the medium-grade metamorphic complex. *International Journal of Earth Sciences* 104, 797-814.
- Cruciani G., Franceschelli M., Jung S., Puxeddu M., Utzeri D., 2008. Amphibole-bearing migmatites from the Variscan Belt of NE Sardinia, Italy: Partial melting of mid-Ordovician igneous sources. *Lithos* 105, 208-224.
- Cruciani G., Franceschelli M., Langone A., Puxeddu M., Scodina M., 2015b. Nature and age of pre-Variscan eclogite protoliths from the Low- to Medium-Grade Metamorphic Complex of north-central Sardinia (Italy) and comparisons with coeval Sardinian eclogites in the northern Gondwana context. *Journal of the Geological Society* 172, 792-807.
- Cruciani G., Franceschelli M., Massonne H.-J., Musumeci G., Spano M.E., 2016. Thermomechanical evolution of the high-grade core in the nappe zone of Variscan Sardinia, Italy: the role of shear deformation and granite emplacement. *Journal of*

- Metamorphic Geology 34, 321-342.
- Cruciani G., Franceschelli M., Musumeci G., Spano M.E., Tiepolo M., 2013. U-Pb zircon dating and nature of metavolcanics and metarkoses from the Monte Grighini Unit: new insights on Late Ordovician magmatism in the Variscan belt in Sardinia, Italy. *International Journal of Earth Sciences* 102, 2077-2096.
- Cruciani G., Franceschelli M., Puxeddu M., Tiepolo M., 2018. Metavolcanics from Capo Malfatano, SW Sardinia, Italy: New insight on the age and nature of Ordovician volcanism in the Variscan foreland zone. *Geological Journal* 53, 1573-1585.
- Cruciani G., Montomoli C., Carosi R., Franceschelli M., Puxeddu M., 2015c. Continental collision from two perspectives: a review of Variscan metamorphism and deformation in northern Sardinia. *Periodico di Mineralogia* 84, 657-699.
- Deer W.A., Howie R.A., Zussman J., 1992. An introduction to the rock-forming minerals. 2<sup>nd</sup> edition, Prentice Hall, Harlow. 696 pp.
- Dostal J. and Chatterjee A.K., 1995. Origin of topaz-bearing and related peraluminous granites of the Late Devonian Davis Lake pluton, Nova Scotia, Canada: crystal versus fluid fractionation. *Chemical Geology* 123, 67-88.
- Dostal J. and Chatterjee A.K., 2000. Contrasting behaviour of Nb/Ta and Zr/Hf ratios in a peraluminous granitic pluton (Nova Scotia, Canada). *Chemical Geology* 163, 207-218.
- El Bouseily A.M. and El Sokkary A.A., 1975. The relation between Rb, Ba and Sr in granitic rocks. *Chemical Geology* 16, 207-219.
- Fancellor D., Cruciani G., Franceschelli M., Massonne H.-J., 2018. Trondhjemitic leucosomes in paragneisses from NE Sardinia: geochemistry and P-T conditions of melting and crystallization. *Lithos* 304-307, 501-517.
- Fettes D. and Desmons J., 2007. Metamorphic rocks - A classification and glossary of terms. Cambridge University Press, Cambridge, 244 pp.
- Flagler P.A. and Spray J.G., 1991. Generation of plagiogranite by amphibolite anatexis in oceanic shear zones. *Geology* 19, 70-73.
- Franceschelli M., Pannuti F., Puxeddu M., 1990. Texture development and PT time path of psammitic schist from the Hercynian chain of NW Sardinia (Italy). *European Journal of Mineralogy* 2, 385-398.
- Franceschelli M., Puxeddu M., Cruciani G., 2005a. Variscan metamorphism in Sardinia, Italy: review and discussion. *Journal of the Virtual Explorer* 19, paper 2.
- Franceschelli M., Puxeddu M., Cruciani G., Dini A., Loi M., 2005b. Layered amphibolite sequence in NE Sardinia, Italy: remnant of a pre-Variscan mafic-silicic layered intrusion? *Contributions to Mineralogy and Petrology* 149(2), 164-180.
- Gaggero L., Oggiano G., Funedda A., Buzzi L., 2012. Rifting and arc-related early Paleozoic volcanism along the north Gondwana margin: Geochemical and geological evidence from Sardinia (Italy). *The Journal of Geology* 120, 273-292.
- Gerlach D.C., Leeman W.P., Lallemand H.G.A., 1981. Petrology and geochemistry of plagiogranite in the Canyon Mountain Ophiolite, Oregon. *Contributions to Mineralogy and Petrology* 77, 82-92.
- Giacomini F., Bomparola R.M., Ghezzi C., Guldbransen H., 2006. The geodynamic evolution of the Southern European Variscides: constraints from the U/Pb geochronology and geochemistry of the lower Palaeozoic magmatic-sedimentary sequences of Sardinia (Italy). *Contributions to Mineralogy and Petrology* 152, 19-42.
- Helbing H. and Tiepolo M., 2005. Age determination of Ordovician magmatism in NE Sardinia and its bearing on Variscan basement evolution. *Journal of the Geological Society* 162, 689-700.
- Koepke J., Berndt J., Feig S.T., Holtz F., 2007. The formation of SiO<sub>2</sub>-rich melts within the deep oceanic crust by hydrous partial melting of gabbros. *Contributions to Mineralogy and Petrology* 153, 67-84.
- Li X.H., Faure M., Lin W., Manatschal G., 2013. New isotopic constraints on age and magma genesis of an embryonic oceanic crust: the Chenaillet Ophiolite in the Western Alps. *Lithos* 160, 283-291.
- Malpas J., 1979. Two contrasting trondhjemitic associations from transported ophiolites in Western Newfoundland: initial report. In: *Developments in Petrology* 6, 465-487. Elsevier.
- Mark G., 1998. Albitite formation by selective pervasive sodic alteration of tonalite plutons in the Cloncurry district, Queensland. *Australian Journal of Earth Sciences* 45, 765-774.
- Massonne H.-J., Cruciani G., Franceschelli M., 2013. Geothermobarometry on anatexitic melts - a high-pressure Variscan migmatite from northeast Sardinia. *International Geology Review* 55, 1490-1505.
- Massonne H.-J., Cruciani G., Franceschelli M., Musumeci G., 2018. Anticlockwise pressure-temperature paths record Variscan upper-plate exhumation: example from micaschists of the Porto Vecchio region, Corsica. *Journal of Metamorphic Geology* 36, 55-77.
- Memmi I., Barca S., Carmignani L., Coccozza T., Elter F.M., Franceschelli M., Gattiglio M., Ghezzi C., Minzoni N., Naud G., Pertusati P.C., Ricci C.A., 1983. Further geochemical data on the pre-Hercynian igneous activities of Sardinia and on their geodynamic significance. In: Sassi F., Szederkényi T. (eds.) *Correlation of Variscan and Pre-variscan events of the Alpine-Mediterranean Mountain belt*. IGCP No 5. Newsletter 5, 87-91.
- Mohammad Y.O., Maekawa H., Ahmmad Lawa F., 2007. Mineralogy and origin of Maekawa albitite from Kurdistan region, northeastern Iraq. *Geosphere* 3, 624-645.
- Montreuil J.F., Corriveau L., Potter E.G., 2015. Formation of albitite-hosted uranium within IOCG systems: the Southern Breccia, Great Bear magmatic zone, Northwest Territories, Canada. *Mineralium Deposita* 50, 293-325.
- Oggiano G., Gaggero L., Funedda A., Buzzi L., Tiepolo M., 2010. Multiple early Paleozoic volcanic events at the northern

- Gondwana margin: U-Pb age evidence from the Southern Variscan branch (Sardinia, Italy). *Gondwana Research* 17, 44-58.
- Pavanetto P., Funedda A., Northrup C.J., Schmitz M., Crowley J., Loi A., 2012. Structure and U-Pb zircon geochronology in the Variscan foreland of SW Sardinia, Italy. *Geological Journal* 47, 426-445.
- Pillola G.L., 1991. Trilobites du Cambrien inférieur du SW de la Sardaigne, Italie. *Palaeontographia Italica* 78, 1-173.
- Polito P.A., Kyser T.K., Stanley C., 2009. The Proterozoic, albitite-hosted, Valhalla uranium deposit, Queensland, Australia: a description of the alteration assemblage associated with uranium mineralisation in diamond drill hole V39. *Mineralium Deposita* 44, 11-40.
- Ricci C.A., Carosi R., Di Vincenzo G., Franceschelli M., Palmeri R., 2004. Unravelling the tectono-metamorphic evolution of medium-pressure rocks from collision to exhumation of the Variscan basement of NE Sardinia: a review. Special issue 2: A showcase of the Italian research in metamorphic petrology. *Periodico di Mineralogia* 73, 73-83.
- Rubatto D. and Hermann J., 2007. Zircon behavior in deeply subducted rocks. *Elements* 3, 31-35.
- Shaw D.M., 1968. A review of K-Rb fractionation trends by covariance analysis. *Geochimica et Cosmochimica Acta* 32, 573-601.
- Singh Y., Viswanathan R., Parihar P.S., Maithani P.B., 2013. X-ray crystallography of uraninites associated with the albitite belt of western India: Evidence for the high-temperature origin of uranium and associated mineralisation. *Journal of the Geological Society of India* 81, 79-90.
- Sun S.S. and McDonough W.S., 1989. Chemical and isotopic systematics of oceanic basalts: implications for mantle composition and processes. Geological Society, London, Special Publications 42, 313-345.
- Turpin L., Maruejol P., Cuney M., 1988. U-Pb, Rb-Sr and Sm-Nd chronology of granitic basement, hydrothermal albitites and uranium mineralization (Lagoa Real, South-Bahia, Brazil). *Contributions to Mineralogy and Petrology* 98, 139-147.
- Wilde A., Otto A., Jory J., MacRae C., Pownceby M., Wilson N., Torpy A., 2013. Geology and mineralogy of uranium deposits from Mount Isa, Australia: implications for albitite uranium deposit models. *Minerals* 3, 258-283.
- Zeng L., Niu H., Bao Z., Shan Q., Li H., Li N., Yang W., 2015. Petrogenesis and tectonic significance of the plagiogranites in the Zhaheba ophiolite, Eastern Junggar orogen, Xinjiang, China. *Journal of Asian Earth Sciences* 113, 137-150.



This work is licensed under a Creative Commons Attribution 4.0 International License CC BY. To view a copy of this license, visit <http://creativecommons.org/licenses/by/4.0/>

